2014

Polarization switching characteristics of 0.5 BaTi0. 8Zr0. 2O3-0.5 Ba0. 7Ca0. 3TiO3 lead free ferroelectric thin films by pulsed laser deposition

Y. D. Kolekar
MSU Graduate Student

A Bhaumik
MSU Graduate Student

P. A. Shaikh

C. V. Ramana

Kartik Ghosh
Missouri State University

Recommended Citation

Kolekar, Y. D., A. Bhaumik, P. A. Shaikh, C. V. Ramana, and K. Ghosh. "Polarization switching characteristics of 0.5 BaTi0. 8Zr0. 2O3-0.5 Ba0. 7Ca0. 3TiO3 lead free ferroelectric thin films by pulsed laser deposition." Journal of Applied Physics 115, no. 15 (2014): 154102.

Polarization switching characteristics of $0.5BaTi_{0.8}Zr_{0.2}O_3$-$0.5Ba_{0.7}Ca_{0.3}TiO_3$ lead free ferroelectric thin films by pulsed laser deposition

Y. D. Kolekar,[1,2,3] A. Bhaumik,[1] P. A. Shaikh,[4] C. V. Ramana,[3] and K. Ghosh[1,a)]
[1]*Department of Physics, Astronomy and Materials Science, Missouri State University, Springfield, Missouri 65897, USA*
[2]*Department of Physics, University of Pune, Pune 411 007, Maharashtra, India*
[3]*Department of Mechanical Engineering, University of Texas at El Paso, El Paso, Texas 79968, USA*
[4]*National Chemical Laboratory (CSIR-NCL), Council of Scientific and Industrial Research, Dr. Homi Bhabha Road, Pashan, Pune 411 008, Maharashtra, India*

(Received 24 February 2014; accepted 5 April 2014; published online 17 April 2014)

We report on the ferroelectricity for morphotropic-phase-boundary lead (Pb) free $0.5BaTi_{0.8}Zr_{0.2}O_3$-$0.5Ba_{0.7}Ca_{0.3}TiO_3$ (0.5BZT-0.5BCT) thin films. Thin films were grown on $Pt/Ti/SiO_2/Si$ substrate using pulsed laser deposition. Raman spectroscopic data combined with the X-ray diffraction analyses confirm body centered tetragonal crystallographic structure 0.5BZT-0.5 BCT thin films on $Pt/Ti/SiO_2/Si$. Polarization studies demonstrate that these 0.5BZT-0.5BCT films exhibit a large remnant and saturation polarization of 37 $\mu C/cm^2$ and 40 $\mu C/cm^2$, respectively, with a coercive field of 140 kV/cm. A correlation between polarization dynamics, structural distortion, and phonon vibration is established. The splitting of X-ray diffraction peak of the thin film in the 2θ range of 44.5° to 46.5° represents high degree of tetragonality. The tetragonality factor calculated by Rietveld analysis was found to be 0.006 and can be a major cause for the increased remnant polarization value. It is established from Raman spectra that the non-centrosymmetricity due to the displacement of Ti/Zr ions from its octahedral position is related to the peak position as well as the broadening of the A_1 (LO) optical phonon mode. This increase of broadness in the thin film causes an increase in the dipole moment of the unit cell and, hence, the net increase in polarization values. © *2014 AIP Publishing LLC*. [http://dx.doi.org/10.1063/1.4871673]

I. INTRODUCTION

Ferroelectric materials with large piezoelectricity exhibit remarkable physical properties, which can be readily integrated into numerous scientific and technological applications such as sensors/actuators used in micro-electro-mechanical systems (MEMS) and transducers.[1–4] Ferroelectric materials also find other high-level technological applications, which include scanning electronic devices, tunable ferroelectric capacitors (FECAP) for non-volatile ferroelectric random access memory (FeRAM), and radio frequency (RF) identification cards.[5–7] For more than half a century, lead (Pb)-based ferroelectrics/piezoelectrics containing morphotropic-phase-boundary (MPB) compositions, viz., lead zirconate titanate (PZT), PMN-PT, and PZN-PT, have been the dominant choice for ferroelectric/piezoelectric based sensor, actuator, and transducer technology.[8] However, these Pb-based materials are currently facing stringent restrictions due to the toxicity of Pb as they contain more than 60% of Pb by weight.[9,10] While there exists a few efforts on the development of Pb-free materials,[11–14] the properties of the reported alternate materials are not the best when compared to the well-known Pb-containing materials. $BaTiO_3$-based ceramics are imperative lead-free piezoelectric ceramics owing to their exceptional dielectric and ferroelectric properties; for example, barium calcium titanate (BCT),[15] barium zirconate titanate (BZT),[16] barium strontium titanate (BST),[17] and so on. However, these materials still do not exhibit very high piezoelectricity or ferroelectricity compared with PZT. Liu and Ren have recently demonstrated that the bulk ceramics of Pb free BZT-BCT system exhibit superior or even better piezoelectric properties, among the reported alternatives to Pb free piezoelectric materials, as compared to the well-known PZT.[18] Enhanced ferroelectric properties, viz., high dielectric constant, high d_{33} values, have been observed in this system close to MPB.[15] An increase in piezoelectricity is the direct consequence of MPB starting from a triple point, which is a tri critical point (TCP) which consequently provides an extremely low energy barrier for polarization rotation and lattice distortion.[15,19] It is essential to fabricate high-quality Pb-free ferroelectric thin films for utilization in practical devices since they are easy for on-chip integration, which is a pre-requisite for incorporation into microelectronic devices.[20,21] Nowadays, there are some reports concerning the fabrication of BZT–xBCT thin films.[22,23] Most are focused on the excellent piezoelectric properties and the structure–properties relationship of this system. Among the different methods, pulsed laser deposition (PLD) technique offers many advantages, such as homogeneity, low-cost, and ability to coat over complex-shaped substrates.[24] This process is more suitable to produce the thin films with the complex compositions of BZT–xBCT. We report on the fabrication of the high-quality Pb-free MPB 0.5BZT-0.5BCT thin films by PLD technique. In addition, a detailed account of the polarization-dynamics, structural-distortion, and phonon-vibration in 0.5BZT-0.5BCT thin films is established.

a)Author to whom correspondence should be addressed. Electronic mail: kartikghosh@missouristate.edu

II. EXPERIMENTAL

A dense ceramic target of 0.5BZT-0.5BCT was made by a standard solid state reaction method using high purity chemicals. The chemicals used were $BaCO_3$ (99.9%, Inframat Advanced Materials), CaO (99.95%, Alfa Aesar), TiO_2 (99.9%, Sigma-Aldrich), and ZrO_2 (99.9%, Inframat Advanced Materials) in required proportions. The final mixture was calcined at 1350 °C and sintered at 1450 °C in air. Thin films of 0.5BZT-0.5BCT were deposited on Pt/Ti/SiO_2/Si substrates by PLD (Excel Instrument, PLD-STD-18) using a 0.5BZT-0.5BCT target. A KrF excimer laser (Lambda Physik, COMPEX 201) with energy density of 2 J cm^{-2}, $\lambda = 248$ nm, pulsed duration of 20 ns, was used at a pulse rate of 10 Hz for the deposition. Thin films were grown by varying growth temperature (from 500 °C to 800 °C) and oxygen pressure (1×10^{-1} mbar to 1×10^{-4} mbar) in the chamber. The best results were obtained at a substrate temperature and pressure of 800 °C and 4×10^{-1} mbar, respectively, during deposition, and subsequently the deposited film was cooled in oxygen pressure of 110 mbar. The base pressure of the deposition chamber was 1.2×10^{-9} bar. Typical film thicknesses were approximately 400 nm measured *ex-situ* by a profilometer (Veeco, Dektak 150). X-ray diffraction (XRD) patterns of both bulk powder and thin film samples were recorded with a X-ray diffractometer (Bruker, D8 Discover) using the θ-2θ scan with CuK_α ($\lambda = 1.5405$ Å). Rietveld fitting was performed on both the bulk powder of 0.5BZT-0.5BCT and PLD grown thin films using DIFFRAC^{plus} TOPAS software. To better analyze the structural data of thin films, XRD data were collected for only the commercially purchased substrate Pt 150 nm (111)/Ti (10 nm)/SiO_2 (300 nm)/Si ⟨100⟩, which was exposed with the same thin film growth (pressure, temperature, and duration) conditions. Using the excitation source of laser with a wavelength of 532 nm, micro-Raman scattering experiments (Horiba, LabRam Raman-PL) were performed in a perfect back-scattering geometry. The Raman spectra were collected in the range of 100 cm^{-1} to 1000 cm^{-1} wave number and the data were analyzed by Gaussian and Lorentzian peak fitting using the Labspec-5 software. For switching and polarization measurements, patterned circular silver top electrodes with a diameter varying from 75 to 200 μm were deposited onto the thin films by RF sputtering. Polarization switching behavior of the films was measured using a virtual ground measurement technique. A function generator (Stanford Research Systems, DS345) supplied a triangle-wave driving voltage of varying amplitude at 1 KHz to the top electrode, and the current response of the sample was obtained through a low noise current preamplifier (Stanford Research Systems, SR 570). Proper filters were used in the low noise current preamplifier to reduce any stray current signals. A storage oscilloscope (Tektronix, TDS420A) in conjunction with Labview 2012 was used to capture voltage-time and current-time data, and Origin Pro 8.5.1 was subsequently employed to calculate the polarization values. The relative dielectric constant and the loss tangent were measured using a precision LCZ meter (Hewlett Packard, 428-4A). The dielectric property measurements at 1 kHz show room-temperature values of the relative dielectric constant ϵ_r and loss tangent tan (∂) of 2240 and 0.04, respectively.

III. RESULTS AND DISCUSSION

A. X-ray diffraction

Figure 1 illustrates the structural quality of 0.5BZT-0.5BCT bulk as well as thin films grown on a Pt/Ti/SiO_2/Si substrate. Figure 1(a) shows the observed XRD pattern (dotted line) along with the calculated (red line) using Rietveld analysis and difference (blue line) profile for the bulk powder sample. The best fit results (goodness of fit = 1.10) are achieved through the consideration of tetragonal structure with the space group symmetry of P4mm. The corresponding refined lattice parameters were found to be $a = 4.005$ Å and $c = 4.019$ Å, which are in accordance with the tetragonal crystallographic structure ($c/a = 1.003$). The XRD pattern recorded for the commercially purchased (111) oriented Pt/Ti/SiO_2/Si substrate alone (Fig. 1(b)) indicates the Pt peaks on the substrate. The Rietveld analysis on the observed XRD data for the grown thin films (Fig. 1(c)) rules out the possibility of impurity phases. No extra peaks were observed in the difference plot except the substrate peaks (Pt peaks were clearly observed in the difference plot). The logarithmic plot (Fig. 1(d)) rules out any possibility of secondary phases present in the thin film. The corresponding refined lattice parameters were found to be $a = 4.001$ Å and $c = 4.026$ Å, which are in accordance with the tetragonal crystallographic structure ($c/a = 1.006$). As the Rietveld analysis of XRD data of 0.5BZT-0.5BCT thin films on Pt/Ti/SiO_2/Si also shows an excellent agreement with the tetragonal structure of P4mm symmetry, the data demonstrate that the 0.5BZT-0.5BCT structure grows very well on the substrate by the PLD process. The increased c/a ratio in the thin film as compared to the bulk corresponds to the structural distortion in the crystal lattice along the c direction in the thin film, which is a cause of the enhanced polarization values. The splitting of XRD peak in the 2θ range of 44.5° to 46.5° is a unique characteristic of tetragonal phase in BZT-xBCT and is quite interesting to investigate. The single (200) plane corresponding to cubic phase transforms to (200) and (002) crystallographic planes, which are the characteristics of a tetragonal structure.[25] The inset XRD plot in Fig. 1(c) proves the presence of tetragonal crystallographic structural symmetry in the PLD grown 0.5BZT-0.5BCT thin film. The asymmetricity of the peak shape indicates the existence of tetragonal and cubic phases. This tetragonal structure might partly be a consequence of averaging ⟨111⟩ displacements of octahedral Ti^{4+} (local rhombohedral structure),[26] although these distortions cannot be conclusively identified from the present results. The splitting of peaks must not be attributed to the presence of CuK_α or CuK_β at higher angles, as this is predominantly seen in the mentioned 2θ range (44.5° to 46.5°).

B. Raman spectroscopy

Raman spectroscopic data collected for 0.5BZT-0.5BCT bulk powder and PLD grown thin films are presented in Fig. 2. Raman spectroscopy data can be used to better understand the mechanism of polarization switching dynamics with molecular vibrational modes present in the crystal lattice. The

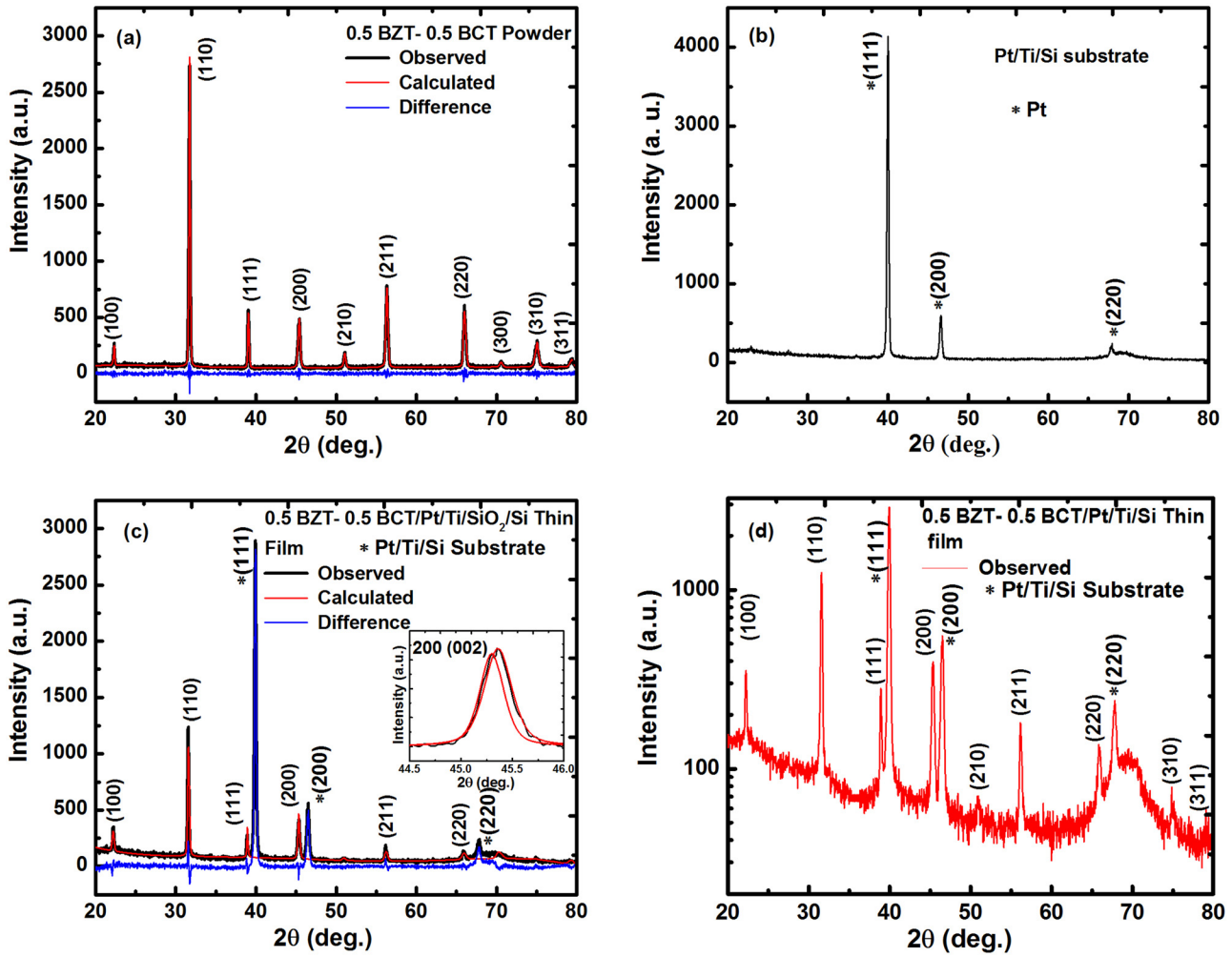

FIG. 1. X-ray diffraction patterns for (a) 0.5BZT-0.5BCT powder sample with the calculated pattern from Rietveld fitting, (b) Pt/Ti/SiO_2/Si only substrate treated with the same growth conditions used for thin film, (c) 0.5BZT-0.5BCT thin film on Pt/Ti/SiO_2/Si substrate with observed and calculated pattern from Rietveld fitting, (d) The logarithmic X-ray diffraction plot for 0.5BZT-0.5BCT thin film confirming the absence of any other secondary phase. The inset plot shows the splitting of (200) peak which a characteristic of the tetragonal crystal structure.

lattice dynamics of ABO_3 type perovskite crystals is illusive in its tetragonal phase and thus attracts considerable attention. For example, tetragonal $BaTiO_3$ with space group P4mm has five atoms and, thus, there are fifteen degrees of freedom present per unit cell.[27] It is well-known that it behaves as a ferroelectric crystal below its transition temperature (T_t) $\sim 120\,^{\circ}C$. The vibrational modes in $BaTiO_3$ are Raman active up to $\sim 120\,^{\circ}C$. The cubic phase above T_t is essentially Raman inactive and can be easily distinguishable from the Raman active tetragonal structure.[18] The Raman active vibrational modes present in 0.5BZT-0.5BCT tetragonal phase are: 2 $A_1(TO) + 1$ $A_1(LO) + 1$ $E(TO) + 1$ $E(LO) + 1$ B_1. Due to the presence of long-range electrostatic forces, each of the A_1 and E modes split into TO (transverse optical) and LO (longitudinal optical) modes.[28–30] The Raman spectrum of 0.5BZT-0.5BCT powder samples shown in Fig. 2(a) exhibits six Raman active modes, which are also present in the PLD grown thin film (Fig. 2(b)). The peaks in both the 0.5BZT-0.5BCT powder/-thin films are observed at 188.9/187.9, 289.0/283.8, 519.0/518.0, and 721.2/743.8, respectively. The peak at 188.9/187.9 cm^{-1} corresponds to the A_1 (TO) mode of vibration.[16] This mode is ascribed to the Ti-O phonon vibrations of 0.5BZT-0.5BCT, while the A_1 (TO) mode at around 519/518 cm^{-1} is due to O-Ti-O symmetric stretching vibrations.[31] The vibrations at 519/518 cm^{-1} are caused due to the presence of non-centrosymmetric regions in which a Ti or Zr atom is displaced from its octahedral position.[32] The sharp feature at 519/518 cm^{-1} for both the powder sample and thin film indicates the high quality of 0.5BZT-0.5BCT. The broad peak for the vibrational mode E (TO)/B_1 is observed at 289.0/283.8 cm^{-1}, which could be due to the Ti-O phonon vibrations and photoluminescence in the sample.[12] In some previous studies on $BaTiO_3$, a sharp peak at 305 cm^{-1} is noticed which signifies its characteristic tetragonal symmetry.[21] However, in our powder and thin film samples, E (2TO) mode of vibration at 305 cm^{-1} becomes negligible which represents substitution of Ti with Zr. The peak position shift towards the left for some vibrational modes in the films could be due to strain in these samples. The peak at 721.2 cm^{-1} in the powder sample is the signature of the tetragonal phase present in the crystallographic structure and corresponds to the A_1(LO)/E(LO) mode of molecular vibrations.[33] The metallic top Pt film used in the present study

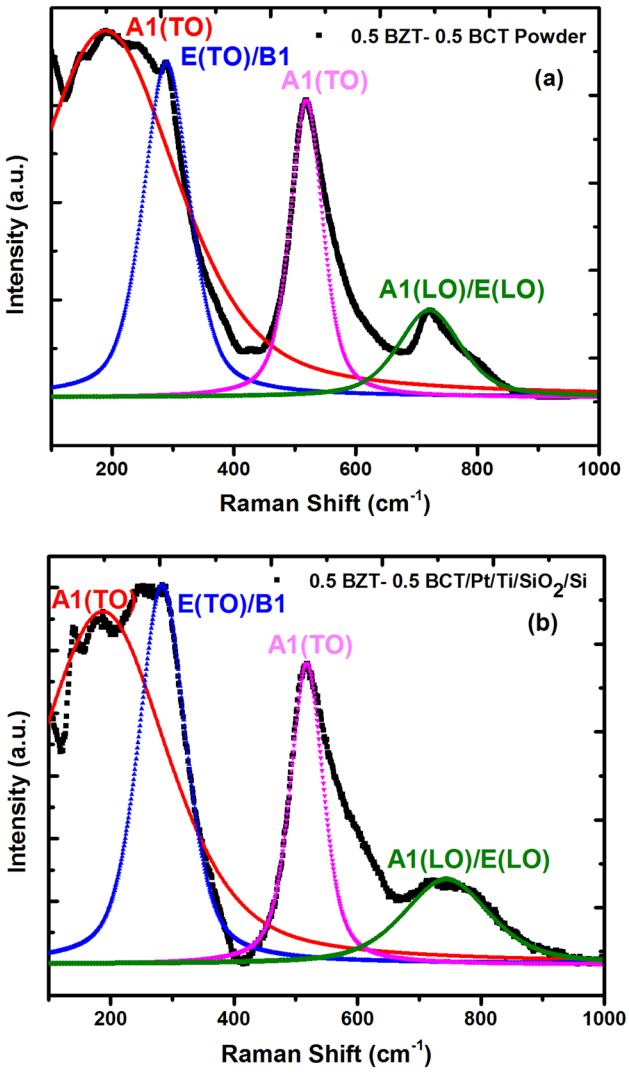

FIG. 2. Raman spectra with Gaussian and Lorentzian single peak fitting by using NSG Labspec software and table showing the peak positions with the FWHM for (a) 0.5BZT-0.5BCT powder, (b) 0.5BZT-0.5BCT thin film on $Pt/Ti/SiO_2/Si$ substrate.

possesses a much lower vibrational frequency to be detected in the Raman spectroscopy. The well-defined peaks in the Raman spectroscopy for the powder and thin film sample prove the presence of high quality samples.

C. Polarization switching

Figure 3 represents the current response with the applied voltage to the FECAP. It can be clearly seen that with the increase in the applied voltage the switching current is predominantly sharper and attains larger values. The sharp feature of the current pulse also rules out the possibility of any leakage current which could enhance the polarization values to be calculated by integrating the current pulse. The time integration of the current response is used for determination of the polarization values. The polarization (P) is calculated using the following relation:

$$P = \frac{Q}{A} = \frac{\int I(t)dt}{A}, \quad (1)$$

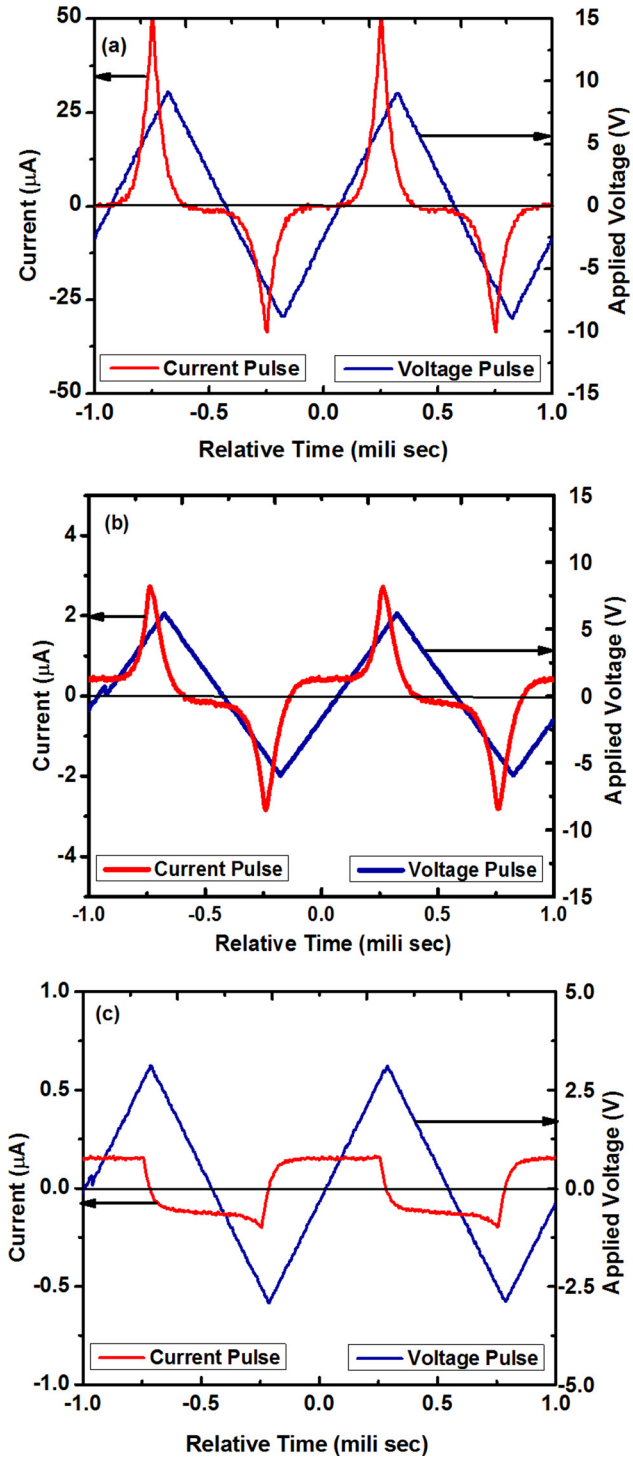

FIG. 3. Switching current-time and applied voltage-time plots at different applied voltages of (a) 9 V, (b) 6 V, and (c) 3 V.

where $I(t)$ is the switching current and A is the area of the top electrode on the FECAP. The area under the peaks is proportional to the total switched polarization and the position of the peak maximum corresponds to the coercive voltage. The asymmetry observed in switching current for two states of polarization represents the imprint in the sample which is a characteristic property of fabricated ferroelectric thin film devices. This suggests that films of ferroelectrics can have unipolar character, strongly preferred polarization direction

in their as-grown state, and that the direction of the unipolarity correlates with the sense of the imprint. Imprint results from trapped charges, charged defects, and other defect dipole complexes, as well as stress gradients.[34,35]

Figure 4(a) represents the I-V characteristics of the thin film. The figure shows a switching current of 50 μA and −38 μA with an applied 9 V in the positive and negative cycles, respectively. The sharpness of the switching current is essential for a superior ferroelectric material. The hysteresis loop is one of the most important tools to characterize ferroelectrics and a significant amount of information can be extracted from the same. Figure 4(b) shows the P-E curves of a 0.5BZT-0.5BCT/Pt/Ti/SiO_2/Si FECAP, which shows a hysteresis loop with a large remnant and saturation polarizations. The P-E curves of the FECAP were obtained by integrating the current-time data for different applied voltages using Origin Pro 8.5.1. The P-E hysteresis loops were centered along the y-axis. As the voltage increases, the FECAP starts to show hysteric characteristics, and saturates at higher voltage. The coercive voltage (V_c) is defined as the voltage where dP/dV reaches maximum, which is approximately 7 V, corresponding to the positive coercive field (E_c) of 140 kV/cm with a small difference in negative direction. The coercive field was dramatically higher than the value of 1.68 kV cm^{-1} for the bulk ceramic counterpart.[18] The much higher coercive field is a consequence of much smaller grains in comparison with the bulk ceramic and hence much more grain boundaries in PLD grown thin film samples.

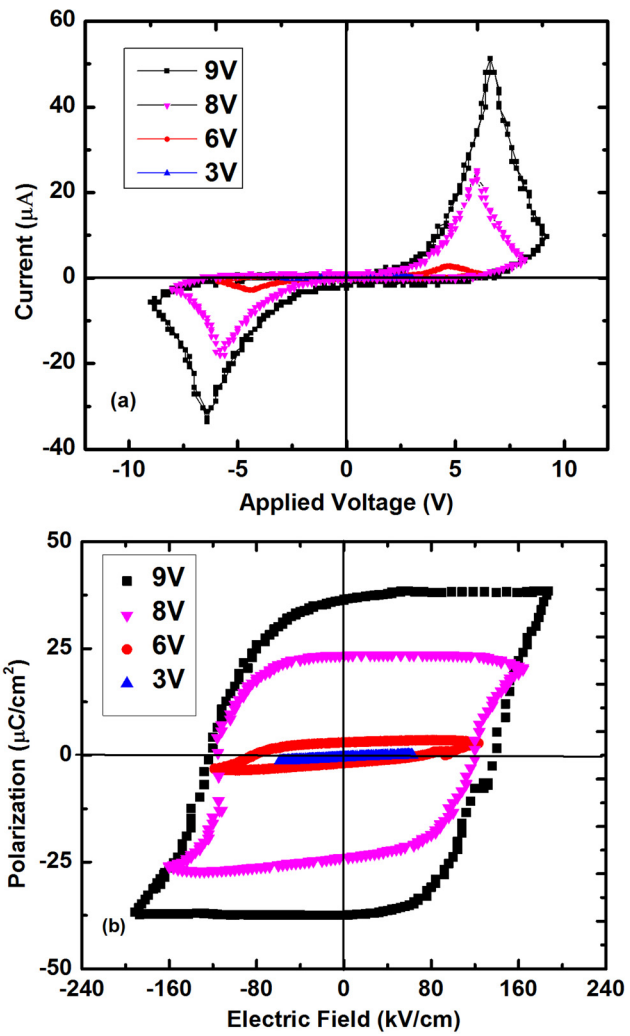

FIG. 4. a) Applied voltage vs. switching current plot at different applied voltages, b) Polarization (P-E) hysteresis loops for ferroelectric capacitors Ag/0.5BZT-0.5BCT/Pt/Ti/SiO_2/Si at different applied voltages.

D. Discussion

The phenomena that account for the observed enhanced remnant and saturation polarization values in 0.5BZT-0.5BCT films, contrast to its bulk sample, can be explained on the basis of observed tetragonal lattice distortion. Evidence can be derived from the XRD data, where *c*/*a* ratio for PLD grown thin film samples is larger than that of corresponding bulk samples. The tetragonality factor (c/a − 1) calculated by Rietveld analysis was found to be 0.006, which is significantly higher than a recent study,[36] and can be a major cause for the increased remnant polarization value. The band at 519/518 cm^{-1} has been observed in both the cubic and tetragonal phases and was conclusively assigned to scattering from the fundamental transverse component of the optical (TO) mode of A1 symmetry.[37] Because first-order Pm3m Raman scattering is symmetry-forbidden in the centrosymmetric space group, the activation of these phonons has been attributed to the presence of non-centrosymmetric regions in which the titanium (zirconium) atom is displaced from the center of the TiO_6 (ZrO_6) octahedra.[32] The weak intensity of the vibration bands of the 0.5BZT–0.5 BCT film, as well as their broadness, is typical of heavily damped phonons. Raman studies indicate that A_1 (TO) mode at ∼519 cm^{-1} and especially A_1 (LO) mode at ∼721.2 cm^{-1} present in our system play a crucial role in the polarization kinetics. We observe a considerable broadening and peak shift of A_1 (LO) vibrational mode, which is a unique feature of the tetragonal phase present in the crystallographic structure. The broadening implies more distortion in the unit cell of the PLD grown films compared to its bulk counterpart. The non-centrosymmetry is related to the peak position as well as the broadening of the A_1 (LO) mode. This increase of broadness in the film due to the displacement of Ti/Zr ions from its octahedral position causes an increase in the dipole moment ($p = q.dl$, where q = charge and dl = distortion) of the unit cell and, hence, the net increase in polarization. The peak positions and full width half max (FWHM) of the corresponding vibrational modes are shown in Table I. The increased value of FWHM for the A_1 (LO) vibrational mode ascertains the enhanced polarization to non-centrosymmetricity of the Ti/Zr ions. Furthermore, superior properties such as large piezoelectricity, enhanced remnant and saturation polarizations of MPB compositions originate from the composition vicinity of the MPB to the tricritical point, which leads to an approximately endangered polarization rotation between the two states of different symmetries, viz., (001) tetragonal (T) and (111) rhombohedral (R) states present in the (1−x)BZT-(x)BCT system.[11] Therefore, simple methodology to attain the enriched ferroelectric and piezoelectric properties is to obtain optimal materials

TABLE I. Peak positions and FWHM of the corresponding vibrational modes observed in Raman Spectroscopy.

Sample name	Vibrational mode(s)/Peak position (cm^{-1})/FWHM (cm^{-1})			
Bulk powder	A1(TO)/188.9/280.5	E(TO)-B1/289.0/90.5	A1(TO)/519.0/63.6	A1(LO)-E(LO)/721.2/121.7
Thin film	A1(TO)/187.9/249.6	E(TO)-B1/283.8/90.7	A1(TO)/518.0/63.9	A1(LO)-E(LO)/743.8/165.0

composition to the proximity of a composition-induced phase transition between two ferroelectric phases. This composition-induced transition, for example, R to T in BZT-xBCT, at MPB causes the instability of the polarization state so that the polarization direction can be easily rotated by external stress or electric field thereby ensuing in a high piezoelectricity, enhanced remnant and saturation polarizations, and permittivity.[38–41] As a theoretical basis, *ab initio* and phenomenological calculations have already revealed that the basic mechanism of the properties enhancement in phase transition regions is flattening of a free energy profile.[19,41,42] The anisotropy of the free energy profile determines easy paths for polarization change and the corresponding properties enhancement.[43] Furthermore, it is important to note that the large piezoelectricity not only requires low polarization anisotropy but also a softening of the lattice.[44] Fortunately, low polarization anisotropy and elastic softening go hand in hand and both contribute to an extraordinary piezoelectricity and enhanced polarization.

IV. CONCLUSION

Summarizing the results, Pb-free and high structural quality thin films of 0.5BZT-0.5BCT close to MPB composition were grown on Pt/Ti/SiO_2/Si substrates using PLD. The Raman spectroscopic data combined with XRD confirm the structural quality of thin films grown on Pt/Ti/SiO_2/Si. Our results demonstrate that PLD grown films of 0.5BZT-0.5BCT close to MPB exhibit an enhanced remnant polarization of 37 $\mu C/cm^2$ and saturation polarization of 40 $\mu C/cm^2$ which are higher than the reported values for BZT-xBCT thin films.[22,23,35] The observed polarization switching characteristics are well-correlated with structural distortion and phonon vibration. The enhanced properties are attributed to the MPB composition, which possesses the low energy barrier between two different polarization states. The results may stimulate and provide a road-map to develop next-generation Pb-free ferroelectric thin films for future non-volatile random access memory applications.

ACKNOWLEDGMENTS

Y. D. Kolekar, one of the authors, acknowledges the Department of Science and Technology, New Delhi, India, for providing financial support through the BOYSCAST fellowship to visit Missouri State University. C.V.R acknowledges with pleasure the support from National Science Foundation (NSF), NSF-PREM Grant No. DMR-1205302. Y.D.K. at UTEP was supported by the AMLIF. We thank Rishi Patel for proof reading this article carefully.

[1]R. Ramesh, *Thin Film Ferroelectric Materials and Devices* (Kluwer Academic Publishers, 1997).
[2]N. B. Gharb, S. T. McKinstry, and D. Damjanovic, J. Appl. Phys. **110**, 124104 (2011).
[3]B. Jaffe, W. R. Cook, Jr., and H. Jaffe, *Piezoelectric Ceramics* (Academic, London, 1971).
[4]S. T. McKinstry and N. B. Gharb, Appl. Phys. Lett. **88**, 202901 (2006).
[5]J. F. Scott, *Ferroelectric Memories* (Springer, 2000).
[6]P. Bintachitt, S. Jesse, D. Damjanovic, Y. Han, I. M. Reaney, S. T. McKinstry, and S. V. Kalinin, Proc. Natl. Acad. Sci. U.S.A. **107**, 7219 (2010).
[7]W. Lee, H. Han, A. Lotnyk, M. A. Schubert, S. Senz, M. Alexe, D. Hesse, S. Baik, and U. Gösele, Nat. Nanotechnol. **3**, 402 (2008).
[8]S.-E. Park and T. R. Shrout, J. Appl. Phys. **82**, 1804 (1997).
[9]E. Aksel and J. L. Jones, Sensors **10**, 1935 (2010).
[10]J. Suchanicz and W. S. Ptak, Ferroelectr. Lett. **12**, 71 (1990).
[11]H. Maiwa, N. Iizawa, D. Togawa, T. Hayashi, W. Sakamoto, M. Yamada, and S.-I. Hirano, Appl. Phys. Lett. **82**, 1760 (2003).
[12]J. Ryu, J.-J. Choi, B.-D. Hahn, D.-S. Park, W.-H. Yoon, and K.-H. Kim, Appl. Phys. Lett. **90**, 152901 (2007).
[13]D. Fu, M. Itoh, S.-Y. Koshihara, T. Kosugi, and S. Tsuneyuki, Phys. Rev. Lett. **100**, 227601 (2008).
[14]R. J. Zeches, M. D. Rossell, J. X. Zhang, A. J. Hatt, Q. He, C.-H. Yang, A. Kumar, C. H. Wang, A. Melville, C. Adamo, G. Sheng, Y. H. Chu, J. F. Ihlefeld, R. Erni, C. Ederer, V. Gopalan, L. Q. Chen, D. G. Schlom, N. A. Spaldin, L. W. Martin, and R. Ramesh, Science **326**, 977 (2009).
[15]L. Y. Li and X. G. Tang, Mater. Chem. Phys. **115**, 507 (2009).
[16]X. G. Tang, K. H. Chew, and H. L. W. Chan, Acta Mater. **52**, 5177 (2004).
[17]Q. X. Liu, X. G. Tang, Y. Y. Deng, J. Wang, and H. L. W. Chan, Mater. Chem. Phys. **112**, 281 (2008).
[18]W. Liu and X. Ren, Phys. Rev. Lett. **103**, 257602 (2009).
[19]H. X. Fu and R. E. Cohen, Nature **403**, 281 (2000).
[20]A. Srivastava, D. Kumar, and R. K. Singh, MRS Proceedings **541**, 41 (1998).
[21]C. W. Nan, M. I. Bichurin, S. Dong, D. Viehland, and G. Srinivasan, J. Appl. Phys. **103**, 031101 (2008).
[22]A. Piorra, A. Petraru, H. Kohlstedt, M. Wuttig, and E. Quandt, J. Appl. Phys. **109**, 104101 (2011).
[23]G. Q. Kang, K. Yao, and J. Wang, J. Am. Ceram. Soc. **95**, 986 (2012).
[24]H. U. Krebs, M. Weisheit, J. Faupel, E. Süske, T. Scharf, C. Fuhse, M. Störmer, K. Sturm, M. Seibt, H. Kijewski, D. Nelke, E. Panchenko, and M. Buback, Adv. Solid State Phys. **43**, 505 (2003).
[25]Y. Shiratori, C. Pithan, J. Dornseiffer, and R. Waser, J. Raman Spectrosc. **38**, 1288 (2007).
[26]K. Page, T. Proffen, M. Niederberger, and R. Seshadri, Chem. Mater. **22**, 4386 (2010).
[27]V. S. Puli, A. Kumar, D. B. Chrisey, M. Tomozawa, J. F. Scott, and R. S. Katiyar, J. Phys. D: Appl. Phys. **44**, 395403 (2011).
[28]P. S. Dobal, A. Dixit, R. S. Katiyar, Z. Yu, R. Guo, and A. S. Bhalla, J. Appl. Phys. **89**, 8085 (2001).
[29]A. Kumar, I. Rivera, and R. S. Katiyar, J. Raman. Spectrosc. **40**, 459 (2008).
[30]G. Burns and F. H. Dacal, Phys. Rev. B **18**, 5750 (1978).
[31]J. C. Sczancoski, L. S. Cavalcante, T. Badapanda, S. K. Rout, S. Panigrahi, V. R. Mastelaro, J. A. Varela, L. M. Siu, and E. Longo, Solid State Sci. **12**, 1160 (2010).
[32]A. Scalabrin, A. S. Chaves, D. S. Shim, and S. P. S. Porto, Phys. Status Solidi B **79**, 731 (1977).
[33]A. Dixit, S. B. Majumder, P. S. Dobal, R. S. Katiyar, and A. Bhalla, Thin Solid Films **284**, 447 (2004).
[34]M. B. Okatan and S. P. Alpaya, Appl. Phys. Lett. **95**, 092902 (2009).
[35]A. Gruverman, B. J. Rodriguez, A. I. Kingon, R. J. Nemanich, J. S. Cross, and M. Tsukada, Appl. Phys. Lett. **82**, 3071 (2003).
[36]Z. Wang, K. Zhao, X. Guo, W. Sun, H. l. Jiang, X. Han, X. Tao, Z. X. Cheng, H. Y. Zhao, H. Kimura, G. Yuan, J. Yin, and Z. G. Liu, J. Mater. Chem. C **1**, 522 (2013).

[37]F. A. Rabuffetti and R. L. Brutchey, J. Am. Chem. Soc. **134**, 9475 (2012).
[38]B. Noheda, D. E. Cox, G. Shirane, S.-E. Park, L. E. Cross, and Z. Zhong, Phys. Rev. Lett. **86**, 3891 (2001).
[39]S. Wada, S. Suzuki, T. Noma, T. Suzuki, M. Osada, M. Kakihana, S.-E. Park, L. E. Cross, and T. R. Shrout, Jpn. J. Appl. Phys., Part 1 **38**, 5505 (1999).
[40]R. Ahluwalia, T. Lookman, A. Saxena, and W. Cao, Phys. Rev. B **72**, 014112 (2005).
[41]Z. G. Wu and R. E. Cohen, Phys. Rev. Lett. **95**, 037601 (2005).
[42]Y. Ishibashi and M. Iwata, Jpn. J. Appl. Phys., Part 1 **38**, 800 (1999).
[43]D. Damjanovic, Appl. Phys. Lett. **97**, 062906 (2010).
[44]M. Iwata, H. Orihara, and Y. Ishibashi, Ferroelectrics **266**, 57 (2002).